Wilson, W. D., Wang, Y.-H., Kusuma, S., Chandrasekaran, S., Yang, N. C., & Boykin, D. W. (1985b) *J. Am. Chem. Soc. 107*, 4989-4995.
Wilson, W. D., Wang, Y.-H., Krishnamoorthy, C. R., & Smith, J. C. (1986) *Chem.-Biol. Interact. 56*, 41-56.
Wilson, W. D., Zuo, E. T., Jones, R. L., Zon, G., & Baumstark, B. R. (1987) *Nucleic Acids Res. 15*, 105-118.
Wu, H.-M., & Crothers, D. S. (1984) *Nature 308*, 509-513.
Xodo, L. E., Manzini, G., Quadrifoglio, F., van der Marel, G. A., & van Boom, J. (1988a) *J. Biomol. Struct. Dyn. 6*, 139-152.
Xodo, L. E., Manzini, G., Quadrifoglio, F., van der Marel, G. A., & van Boom, J. (1988b) *Biochemistry 27*, 6321-6326.
Yoon, C., Prive, G. G., Goodsell, D. S., & Dickerson, R. E. (1988) *Proc. Natl. Acad. Sci. U.S.A. 85*, 6332-6336.

NMR Studies of an Exocyclic 1,N^2-Propanodeoxyguanosine Adduct (X) Located Opposite Deoxyadenosine (A) in DNA Duplexes at Basic pH: Simultaneous Partial Intercalation of X and A between Stacked Bases†

Michael Kouchakdjian,‡ Moises Eisenberg,§ David Live,∥ Edmund Marinelli,§ Arthur P. Grollman,*,§ and Dinshaw J. Patel*,‡

Department of Biochemistry and Molecular Biophysics, College of Physicians and Surgeons, Columbia University, New York, New York 10032, Department of Pharmacological Sciences, State University of New York at Stony Brook, Stony Brook, New York 11794, and Chemistry Department, Emory University, Atlanta, Georgia 30322

Received September 12, 1989; Revised Manuscript Received November 29, 1989

ABSTRACT: The NMR parameters for the 1,N^2-propanodeoxyguanosine (X) opposite deoxyadenosine positioned in the center of the complementary d(C1-A2-T3-G4-X5-G6-T7-A8-C9)·d(G10-T11-A12-C13-A14-C15-A16-T17-G18) X·A 9-mer duplex are pH dependent. A previous paper established protonated X5(syn)·A14(anti) pairing in the X·A 9-mer duplex at pH 5.8 [Kouchakdjian, M., Marinelli, E., Gao, X., Johnson, F., Grollman, A., & Patel, D. J. (1989) *Biochemistry 28*, 5647-5657]; this paper focuses on the pairing alignment at the lesion site at pH 8.9. The observed NOEs between specific exocyclic CH_2 protons and both the imino proton of G6 and the sugar H1′ protons of C13 and A14 establish that X5 is positioned toward the G6·C13 base pair with the exocyclic ring directed between C13 and A14 on the partner strand. The observed NOE between the H2 proton of A14 and the imino proton of G4, but not G6, establishes that A14 at the lesion site is directed toward the G4·C15 base pair. NOEs are detected between all exocyclic CH_2 protons of X5 and the H2 proton of A14, confirming that both X5 and A14 are directed toward the interior of the helix. The X5(anti)·A14(anti) alignment at pH 8.9 is accommodated within the helix with retention of Watson-Crick pairing at flanking G4·C15 and G6·C13 base pairs. The energy-minimized conformation of the (G4-X5-G6)·(C13-A14-C15) segment at pH 8.9 establishes that X5 and A14 are directed into the helix, partially stack on each other, and are not stabilized by intermolecular hydrogen bonds. The X5 base is partially intercalated between C13 and A14 on the unmodified strand, while A14 is partially intercalated between G4 and X5 on the modified strand. This results in a larger separation between the G4·C15 and G6·C13 base pairs flanking the lesion site in the basic pH conformation of the X·A 9-mer duplex. The midpoint of the transition between the protonated X5(syn)·A14(anti) and X5(anti)·A14(anti) conformations occurs at pH 7.6, establishing an unusually high pK_a for protonation of the A14 ring opposite the X5 exocyclic adduct site. Thus, the interplay between hydrophobic and hydrogen-bonding contributions modulated by pH defines the alignment of 1,N^2-propanodeoxyguanosine opposite deoxyadenosine in the interior of DNA helices.

There is currently very little known at the molecular level about structural features of nucleic acid exocyclic adducts important in mutagenesis and carcinogenesis (Shapiro, 1969; Singer & Grunberger, 1983; Singer & Bartsch, 1986; Basu & Essigmann, 1988). The formation of these adducts not only interferes with base-pairing regions in nucleic acid components but also induces substantial alterations in pK_a and hydrophobicity at the lesion site. There is a potential for local helix distortion at sites of exocyclic adduct formation, which may exert substantial effects on DNA replication and repair and lead ultimately to mutagenesis and carcinogenesis.

Exocyclic adducts may be generated through Michael addition of α,β-unsaturated carbonyl compounds to the N1 and N2 positions of deoxyguanosine followed by ring closure. Our studies have focused on the 1,N^2-propanodeoxyguanosine adduct **1** (Marinelli et al., 1990), which is a stable analogue of the adduct generated with acrolein but lacking the hydroxyl group (Chung et al., 1984). We have inserted exocyclic adduct **1** into DNA oligonucleotide duplexes in order to determine the structural and biological consequences of the additional ring in the adduct with the goal of elucidating the molecular basis of the mutagenic potential of exocyclic adducts.

Biological studies in vivo and in vitro have shown that upon replication, deoxyadenosine is incorporated preferentially opposite 1,N^2-propanodeoxyguanosine (Grollman, 1989).

† This research was supported by NIH CA-49982 to D.J.P. and NIH CA-47995 to A.P.G. NMR studies were conducted on instruments purchased with funds provided by the Robert Woods Johnson Jr. Charitable Trust and Matheson Foundation.
‡ Columbia University.
§ State University of New York at Stony Brook.
∥ Emory University.

0006-2960/90/0429-4456$02.50/0

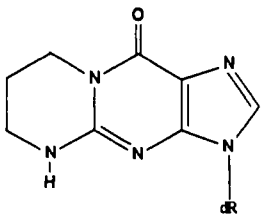

1

C1-A2-T3-G4-X5-G6-T7-A8-C9
G18-T17-A16-C15-A14-C13-A12-T11-G10

2

We have undertaken two-dimensional proton NMR and energy minimization studies on the d(C1-A2-T3-G4-*X5*-G6-T7-A8-C9)·d(G10-T11-A12-C13-*A14*-C15-A16-T17-G18) nonanucleotide duplex (designated X·A 9-mer, **2**), which contains a 1,N^2-propanodeoxyguanosine exocyclic adduct, X5, opposite deoxyadenosine A14 in the center of the helix. Previous NMR studies have established formation of a protonated X5(syn)·A14(anti) pair in the X·A 9-mer duplex at pH 5.8 in aqueous solution (Kouchakdjian et al., 1989). The alignment of X5 and A14 is dependent on pH and the present study investigates the X5·A14 lesion site at pH 8.9.

The distance bounds obtained from NOESY data sets have been included as constraints to generate energy-minimized structures of the full X·A 9-mer duplex at pH 5.8 and at pH 8.9.

Experimental Procedures

Oligonucleotide Synthesis. The synthesis, isolation, and purification of 1,N^2-(1,3-propano)-2′-deoxyguanosine (**1**) generated by reaction of 1,3-dibromopropane with deoxyguanosine in dimethyl sulfoxide was reported previously (Marinelli et al., 1990). The 5′-*O*-dimethoxytrityl (DMT) ether of **1** and the further derived 3′-*O*-[(*N*,*N*-diisopropylamino)-β-cyanoethoxy]phosphoramidite were prepared by standard methods and displayed spectral data that confirmed their structures.

The desired oligodeoxynucleotides were assembled on 5 μmol of resin by employing a Du Pont Codex 300 automated DNA synthesizer, the above phosphoramidite being added manually in a normal coupling reaction. The isolation, deprotection, and purification of the modified and unmodified strands of the X·A 9-mer duplex have been reported previously (Kouchakdjian et al., 1989).

Sample Preparation. The addition of equimolar amounts of the modified and unmodified strands was monitored by measuring the intensities of the deoxyadenosine H8 and H2 resonances and the thymidine CH_3 resonances at high temperature. The NMR experiments were performed on 250 A_{260} units of X·A 9-mer duplex in 0.4 mL of 0.1 M NaCl, 10 mM phosphate, 1 mM EDTA in either 100% D_2O or in 90% H_2O–10% D_2O (v/v). The pH values in D_2O are uncorrected pH meter readings.

NMR Experiments. Proton NMR experiments were recorded on a Bruker AM 500 spectrometer and are referenced relative to external 3-(trimethylsilyl)propionate-*2,2,3,3-d*$_4$ (TSP). Two-dimensional phase-sensitive proton NOESY spectra in H_2O were recorded by using a jump and return (90_y, τ, 90_{-y}) detection pulse. Preparation and mixing pulses were 70° hard pulses and the mixing time was 120 ms (1.0-s repetition delay). The carrier frequency was centered on the H_2O signal and the waiting time was optimized so that the imino and aromatic protons were equally excited. Two-dimensional phase-sensitive proton NOESY spectra in D_2O were collected with a repetition delay of 1.5 s and mixing times of 50 and 300 ms. The residual HOD resonance was presaturated by using the decoupler channel. The data accumulation and processing parameters for NOESY data sets in H_2O and D_2O solution have been outlined previously (Kouchakdjian et al., 1989). The data sets were processed using FT-NMR on a μVAXII computer.

Phase-sensitive two-dimensional proton-detected phosphorus–proton COSY spectra were recorded with 5-mm proton reverse detection and a broad-band decoupler accessory on the GN 500 spectrometer. The pulse sequence in the heteronuclear two-dimensional experiments was described previously (Sklenar et al., 1986) except for the receiver phase cycling, which should be corrected to sequence B in Sklenar and Bax (1987). The acquisition and processing parameters are similar to those reported previously (Norman et al., 1989). Chemical shifts were referenced relative to trimethyl phosphate (TMP) in D_2O indirectly based on a measurement of a sample of TMP and TSP in D_2O, and following the procedure for relating proton standard positions to that of another nucleus as described elsewhere (Live et al., 1984).

Distance Constraints. The interproton distances were estimated from the volume integrals of cross peaks in the NOESY spectra of the X·A 9-mer in D_2O at pH 5.8 (50 and 250 ms mixing times) and pH 8.9 (50 and 300 ms mixing times). These distances were derived from the relationship

$$\frac{\eta_{ij}}{\eta_{kl}} = \frac{(r_{kl})^6}{(r_{ij})^6}$$

where r_{ij} is the unknown distance, r_{kl} is the fixed internal reference distance (cytidine H5–H6 distance of 2.45 Å), and η_{ij} and η_{kl} are the volume integrals of the corresponding cross peaks. The unknown distances are defined by broad lower and upper bounds since the constraints are based on one short (50 ms) and one long (250 or 300 ms) mixing time and spin diffusion contributes at the longer mixing time.

Starting Models. Standard B-DNA nucleotides from the molecular modeling program Macromodel (Prof. W. C. Still, Columbia University) were used to construct the 1,N^2-propanodeoxyguanosine exocyclic adduct containing X·A 9-mer duplex. The deoxyguanosine base at position 5 was modified to incorporate the propano bridge to generate the 1,N^2-propanodeoxyguanosine.

The glycosidic torsion angles of X5 and A14 are in the anti orientation for the starting model of the X·A 9-mer at pH 8.9, and this results in the initial model having a clash of the X5 and A14 bases in the center of the helix.

The glycosidic torsion angle of X5 is syn and of A14 is anti for the starting model of the X·A 9-mer at pH 5.8. Furthermore, the N1 position is protonated for A14 as established in the experimental data (Kouchakdjian et al., 1989).

Minimization. The energy minimization of the starting models of the entire X·A 9-mer duplexes at pH 8.9 and at pH 5.8 were carried out using the program XPLOR (Prof. A. Brunger, Yale University) on an Alliant FX1 minisupercomputer. We took 5000 steps using the conjugate gradient algorithm to reach a stable conformation. NOE-determined distances were incorporated as constraints by use of the square-well potential approximation with a scale factor of 3. The base pairs flanking the lesion were further constrained with square-well potentials to maintain Watson–Crick pairing

Table I: Proton Chemical Shifts in X·A 9-mer, pH 8.9

	exchangeable proton chemical shifts, 2 °C (ppm)				
base pair	T-H3	G-H1	C-H4b	C-H4e	A-H2
C1·G18					
A2·T17	13.65				7.80
T3·A16	13.65				7.80
G4·C15		12.36	8.22	6.82	
X5·A14					7.60
G6·C13		12.33	8.00	6.67	
T7·A12	13.47				7.47
A8·T11	13.60				7.55
C9·G10					

	nonexchangeable proton chemical shifts, 8 °C (ppm)						
	H8	H2	H6	H5/CH_3	H1′	H2′, H2″	H3′
C1			7.67	5.88	5.59	2.01, 2.42	4.70
A2	8.42	7.82			6.29	2.75, 2.92	5.04
T3			7.07	1.41	5.69	1.63, 2.09	4.80
G4	7.80				5.91	2.52, 2.62	4.77
X5	7.61					2.22, 2.39	
G6	7.92				5.95	2.78, 2.86	
T7			7.27	1.43	5.63	2.16, 2.44	
A8	8.25	7.59			6.26	2.66, 2.87	5.04
C9			7.23	5.05	5.99	2.10, 2.15	
G10	7.88				5.91	2.63, 2.76	4.79
T11			7.39	1.34	5.74	2.16, 2.47	
A12	8.28	7.50			6.20	2.67, 2.85	5.04
C13			7.24	5.33	5.75	1.85, 1.97	4.74
A14	8.17	7.62			5.95	2.50, 2.61	4.87
C15			7.65	5.74	5.74		
A16	8.40	7.82			6.29	2.77, 2.94	5.06
T17			7.14	1.52	5.78	1.86, 2.29	4.83
G18	7.86				6.11	2.34, 2.60	4.67

characteristic of B-form DNA. Electrostatic potential energy terms were based on a fully charged set of partial charges (−1/residue, −2 for A14 at pH 5.8) using a dielectric constant of 80.

Results

Proton Spectra. The exchangeable proton (6–14 ppm), the nonexchangeable proton (5.5–9.0 ppm), and the backbone phosphorus (−2.8 to −5.2 ppm) spectra of the X·A 9-mer duplex in 0.1 M NaCl, 10 mM phosphate, aqueous solution, pH 8.9, are plotted in Figure 1, parts A–C, respectively. These spectra establish that the X·A 9-mer duplex adopts a single conformation at pH 8.9 that is distinctly different from the unique conformation of the X·A 9-mer duplex at pH 5.8 reported previously (Kouchakdjian et al., 1989). These two conformations are at equilibrium and are reversible upon pH variation. The exchange equilibrium between the acidic and basic pH conformations is slow on the NMR time scale since resonances from both states are detected at intermediate pH values.

This contribution focuses on the conformation of the X·A 9-mer duplex at pH 8.9. Furthermore, this high-pH form is contrasted with the low-pH form of the X·A 9-mer duplex at pH 5.8, which was previously characterized by us (Kouchakdjian et al., 1989).

Exchangeable Protons. The exchangeable proton spectrum of the X·A 9-mer duplex in H_2O buffer, pH 8.9 at 5 °C (Figure 1A), displays a somewhat broadened imino proton region due to both low temperature and exchange catalysis at basic pH. The phase-sensitive NOESY spectrum (120-ms mixing time) of the X·A 9-mer duplex in H_2O buffer, pH 8.9, has been recorded at 2 °C with expanded regions plotted in Figure 2.

The imino protons may be assigned to specific base pairs in the X·A 9-mer at pH 8.9 on the basis of the observed cross peaks between adjacent A·T and G·C base pairs (peaks A and B, Figure 2A), between thymidine imino and adenosine H2 protons within A·T pairs (peaks C–E, Figure 2B), and between guanosine imino and cytidine amino protons within G·C pairs (peaks F and G, peaks H and I, Figure 2B). Thus, NOEs are detected between the imino protons of adjacent G6·C13 and T7·A12 base pairs (peak B, Figure 2A) and T3·A16 and G4·C15 base pairs (peak A, Figure 2A). These assignments are used to determine the alignment of bases across the A·T and G·C pairs. The overlapping imino protons of T3 and T17 display a NOE to the adenosine H2 protons of A16 and A2, respectively (peak C, Figure 2B), while the imino protons of T11 and T7 show cross peaks to the H2 protons of A8 (peak D, Figure 2B) and A12 (peak E, Figure 2B), respectively. The base pairs immediately flanking the exocyclic lesion are fully paired, as reflected in the NOEs between the imino proton of G4 and the amino protons of C15 (peaks F and G, Figure 2B) of the G4·C15 pair on one side of the exocyclic lesion and the imino proton of G6 and the amino protons of C13 (peaks H and I, Figure 2B) of the G6·C13 pair on the other side. A NOE is detected between the adenosine H2 of A16 and the imino proton of G4 (peak J, Figure 2B) on adjacent T3·A16 and G4·C15 base pairs.

Additionally, a NOE is detected between the adenosine H2 proton of A14 at the lesion site and the imino proton of G4 (peak K, Figure 2B) of the flanking G4·C15 base pair. A relatively weak NOE is detected between the imino proton of G6 and the 1.66 ppm CH_2 proton of the propano bridge of the adjacent exocyclic base (X5) (peak M, Figure 2C). The presence of this NOE was confirmed by a one-dimensional NOE difference experiment (Figure S1, supplementary material).

The chemical shifts of the imino and amino protons and the adenosine H2 protons in the X·A 9-mer duplex in H_2O buffer, pH 8.9, at 2 °C are tabulated in Table I.

Nonexchangeable Protons. The phase-sensitive NOESY (300-ms mixing time) spectrum of the X·A 9-mer duplex in D_2O buffer, pH 8.9, 8 °C (Figure S2, supplementary material), exhibits well-resolved NOE cross peaks permitting assignment of the nonexchangeable base and sugar protons. An expanded region of this NOESY contour plot depicting the NOE cross peaks between the base protons and the sugar H1′ and cytidine H5 protons is plotted in duplicate in Figure 3. The NOE cross peaks link the base (purine H8 and pyrimidine H6) protons with their own and 5′-flanking sugar H1′ protons.

Table II: Proton Chemical Shift Differences in the X·A 9-mer Duplex between pH 5.8 and pH 8.9[a]

	chemical shift difference (ppm)								
	NH1	H8	H2	NH4	H6	H5/CH_3	H1′	H2′,H2″	H3′
G4	0.13	0.06					0.07	0.08, −0.29	0.15
X5		0.15						−0.29, −0.75	
G6	−0.22	0.11					0.20	0.52, 0.28	
C13				−0.11, −0.25	−0.11	−0.01	0.41	−0.22, −0.36	
A14		−0.30	−0.40				−0.34	−0.19, −0.37	−0.17
C15				0.08, 0.03	0.33	0.40	0.24		

[a] Positive and negative values correspond to downfield and upfield chemical shifts, respectively, on proceeding from pH 5.8 to pH 8.9.

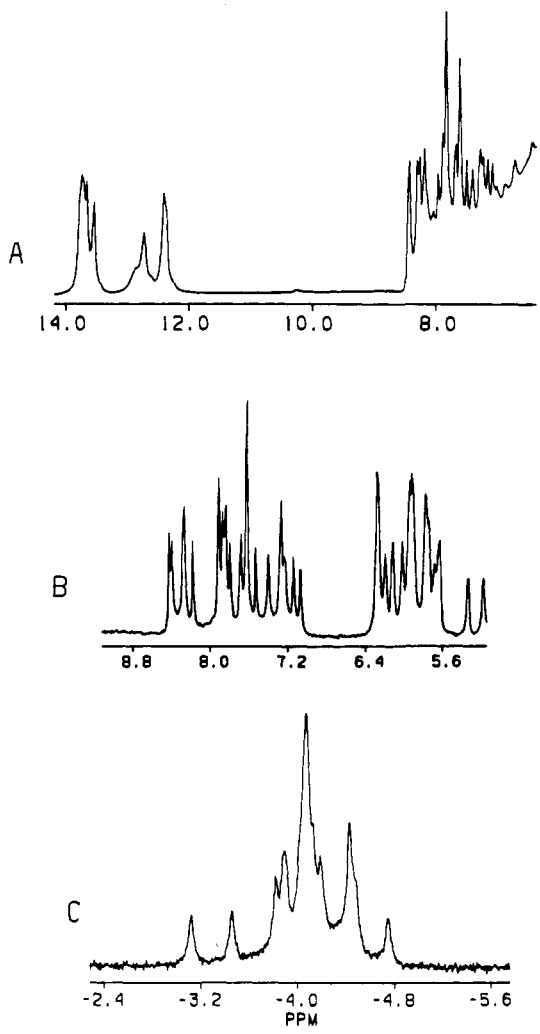

FIGURE 1: NMR spectra of the X·A 9-mer duplex in 0.1 M NaCl, 10 mM phosphate, aqueous solution, pH 8.9. (A) Exchangeable 500-MHz proton spectra (6.5–14.0 ppm) in H_2O buffer, 0 °C. (B) Nonexchangeable 500-MHz proton spectra (5.2–8.8 ppm) in D_2O buffer, 15 °C. (C) Proton-decoupled 121-MHz phosphorus spectra (−2.8 to −5.2 ppm) in D_2O buffer, 15 °C.

Table III: Proton Chemical Shifts of Exocyclic CH_2 Protons in the X·A 9-mer Duplex at pH 5.8 and pH 8.9

	chemical shift (ppm)	
	pH 5.8	pH 8.9
central CH_2	1.85, 2.00	1.22, 1.22
flanking CH_2	3.35, 3.35, 3.53, 3.65	1.84, 2.67, 2.87, 3.06

The deoxynucleotide chain can be traced with interruptions from C1 to C9 in the modified strand (Figure 3A) and from G10 to G18 in the unmodified strand (Figure 3B). It was not possible to fully trace the chain in the G4-X5-G6 (Figure 3A) and C13-A14-C15 (Figure 3B) segments due to spectral overlap in the ~7.65 ppm region (superposition of H6 of C1, H6 of C15, H8 of X5, and H2 of A14). This problem of spectral overlap centered at the ~7.65 ppm region was resolved by editing out the strong cross peaks due to the H5 and H6 protons of C1 (peak C1*, Figure 3A) and C15 (peak C15*, Figure 3B). This was achieved by replacing the H5 protons of both C1 and C15 by CH_3 groups. Thus, the intense NOE due to the H5–H6 coupling would disappear from the base to sugar H1′ proton region and fall in the base to methyl region on replacement of C1 and C15 by ^{5}meC1 and ^{5}meC15 in the X·A 9-mer duplex. The NOESY spectrum of the X·A 9-mer duplex at pH 8.9 containing the ^{5}meC1 and ^{5}meC15 bases was

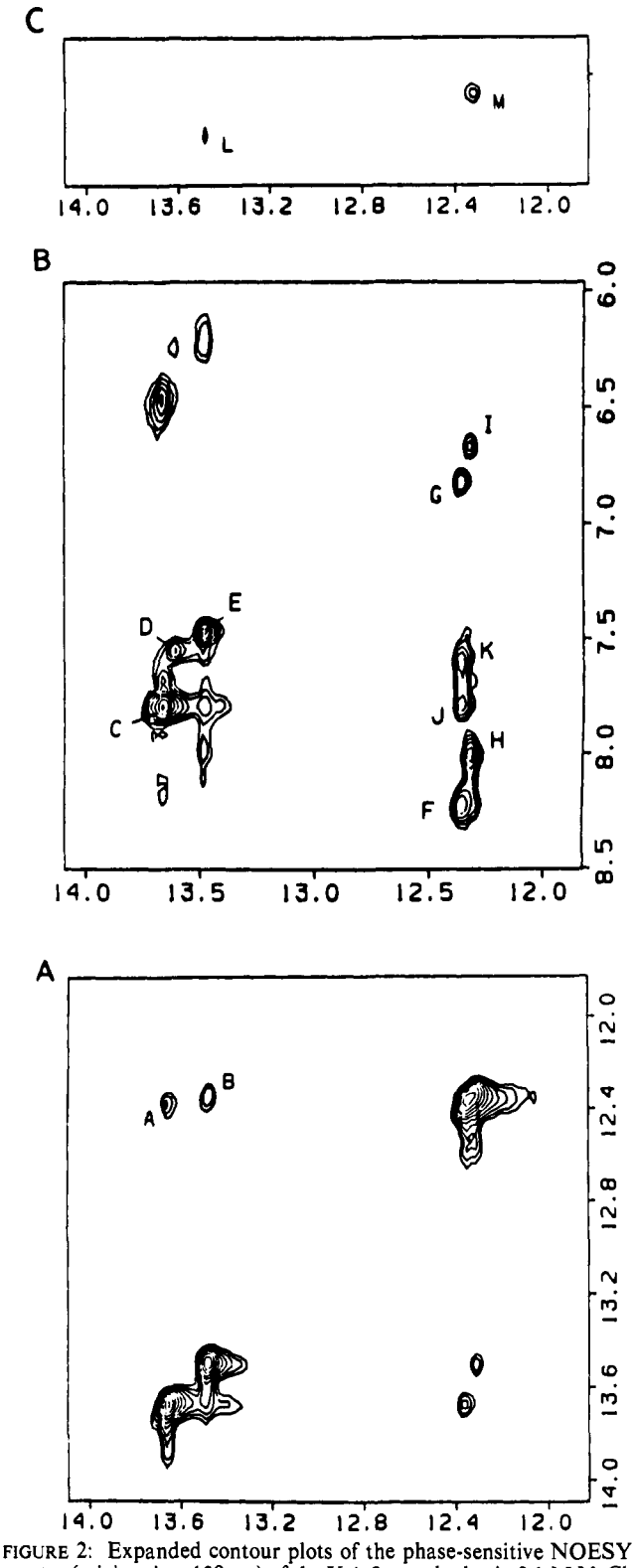

FIGURE 2: Expanded contour plots of the phase-sensitive NOESY spectra (mixing time 120 ms) of the X·A 9-mer duplex in 0.1 M NaCl, 10 mM phosphate, H_2O, pH 8.9, 2 °C. (A) Cross peaks establishing connectivities in the symmetrical 12.0–14.0 ppm imino proton region. (B) Cross peaks establishing connectivities between 12.0–14.0 ppm imino proton and the 6.0–8.5 ppm base and amino proton region. (C) Cross peaks establishing connectivities between the 12.0–14.0 ppm imino proton region and the 1.0–1.6 ppm region. The cross peaks A–M are discussed in the text.

recorded and the corresponding contour plot relating the base to the sugar H1′ and the cytidine H5 region is shown in duplicate in Figures 4, parts A and B. The resulting simplification of the spectrum greatly aided the determination of the assignments of the NOE cross peaks in question.

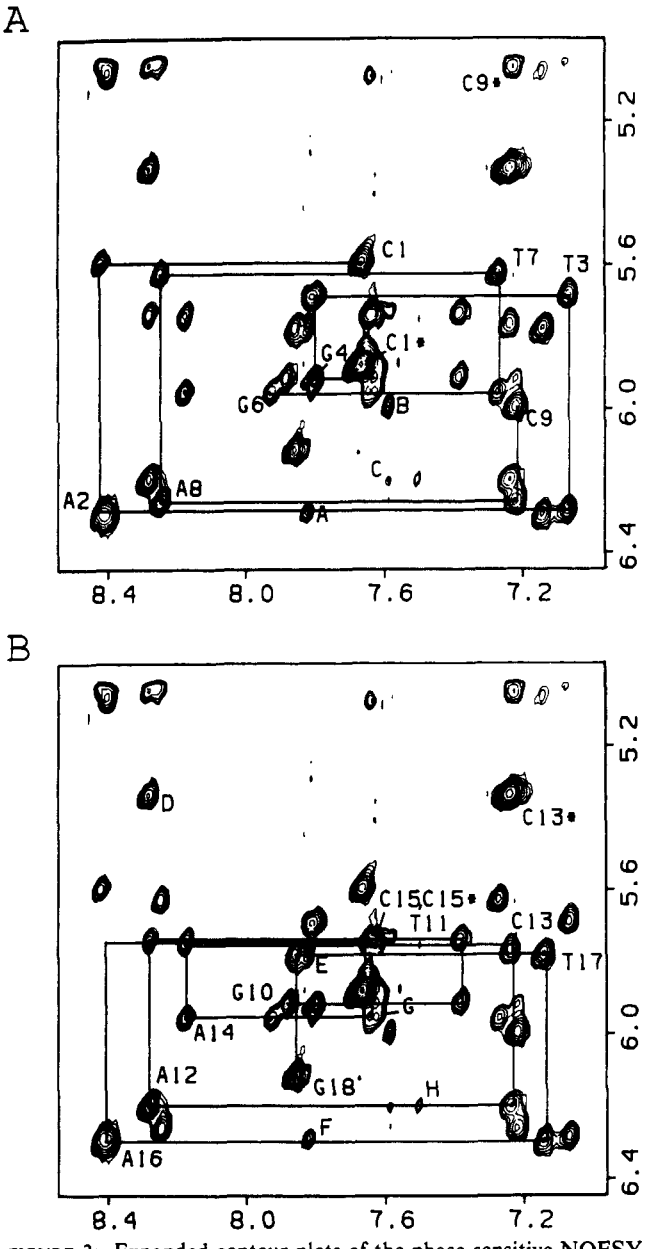

FIGURE 3: Expanded contour plots of the phase-sensitive NOESY spectrum (mixing time 300 ms) of the X·A 9-mer duplex in 0.1 M NaCl, 10 mM phosphate, D_2O, pH 8.9, at 8 °C establishing distance connectivities between the base protons (7.0–8.5 ppm) and the sugar H1′ and deoxycytidine H5 protons (5.0–6.4 ppm). The chain is traced from C1 to C9 in (A), and the chain is traced from G10 to G18 in (B). The tracing follows connectivities between adjacent base protons through their intervening sugar H1′ protons. The deoxycytidine H5–H6 connectivities are designated by asterisks. The assignments of NOE cross peaks A–H are listed below. (A) A2(H2) to A2(H1′), (B) A8(H2) to C9(H1′), (C) A8(H2) to A12(H1′), (D) A12(H8) to C13(H5), (E) A16(H2) to T17(H1′), (F) A16(H2) to A16(H1′), (G) A14(H2) to A14(H1′), (H) A12(H2) to A12(H1′).

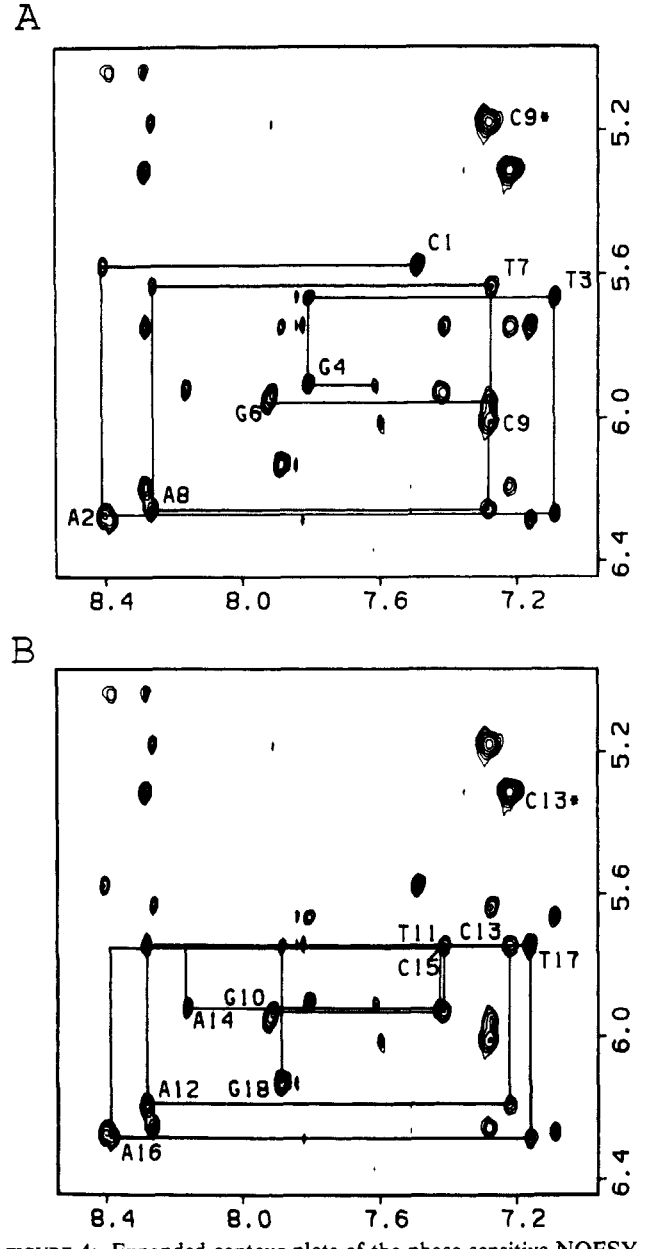

FIGURE 4: Expanded contour plots of the phase-sensitive NOESY spectrum (mixing time 300 ms) of the X·A 9-mer duplex (labeled with 5-methyldeoxycytidine at C1 and C15) in 0.1 M NaCl, 10 mM phosphate, D_2O, pH 8.9, at 8 °C establishing distance connectivities between the base protons (7.0–8.5 ppm) and the sugar H1′ and deoxycytidine H5 protons (5.0–6.4 ppm). The chain is traced from C1 to C9 in (A), and the chain is traced from G10 to G18 in (B).

There are several NOE cross peaks that are either missing or too weak to detect in the (G4-X5-G6)·(C13-A14-C15) segment centered about the X5·A14 lesion site in the expanded NOESY plots of the ^{5}meC-modified X·A 9-mer duplex, pH 8.9, in Figure 4, parts A and B. The missing NOE cross peaks correspond to distance connectivities between the H8 and H1′ protons of X5 (Figure 4A), between the H8 of G6 and the H1′ of X5 (Figure 4A), and between the H8 of A16 and the H1′ of C15 (Figure 4B).

The 300- and 50-ms mixing time NOESY stacked plots of the X·A 9-mer at pH 8.9 are plotted in Figure S3, parts A and B, respectively (supplementary material). The intensities of the NOEs from the base to their own sugar H1′ protons are weak relative to the intensities of the NOEs between the cytidine H5 to H6 protons (Figure S3).

The distance connectivities between the base protons (7.0–8.6 ppm) and the sugar H2′,H2″ protons are shown in an expanded plot of the X·A 9-mer at pH 8.9 in Figure 5A. The cross peaks are partially resolved and establish that the NOEs between the H8 of G6 and the H2′,H2″ protons of X5 and between the H6 of C15 and the H2′,H2″ protons of A14 are either absent or too weak to be detected.

The NOEs between the base protons and the methylene protons of the propano bridge of the exocyclic base also fall in this region. These resolved CH_2 protons of X5 resonate at 1.22 (two superpositioned peaks), 1.84, 2.67, 2.87, and 3.06 ppm (Figure 5C). All the X5 methylene protons show NOE cross peaks to the H2 proton of A14 (boxed peaks, Figure 5A). Furthermore, the exocyclic CH_2 protons at 1.22 ppm exhibit

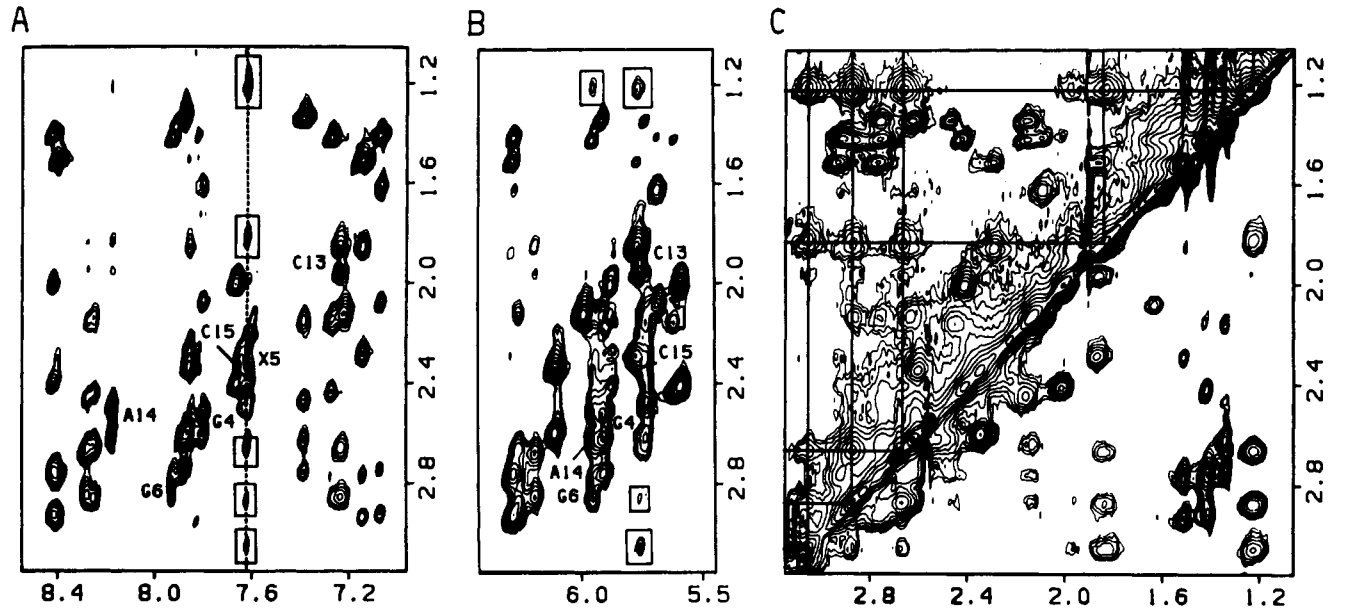

FIGURE 5: Expanded contour plots of the phase-sensitive NOESY spectra (mixing time 300 ms) of the X·A 9-mer duplex in 0.1 M NaCl, 10 mM phosphate, D_2O, pH 8.9, at 8 °C. (A) Cross peaks establishing distance connectivities between the base protons (7.0–8.5 ppm) and the sugar H2′,H2″ and exocyclic CH_2 protons (1.0–3.0 ppm). The assignments list NOEs between base protons and their own sugar H2′,H2″ protons in the (G4-X5-G6)·(C13-A14-C15) segment. The boxed peaks are discussed in the text. (B) Cross peaks establishing distance connectivities between the sugar H1′ protons (5.5–6.4 ppm) and the sugar H2′,H2″ and exocyclic CH_2 protons (1.0–3.0 ppm). The assignments list NOEs between sugar H1′ and their own sugar H2′,H2″ protons in the (G4-X5-G6)·(C13-A14-C15) segment. The boxed peaks are discussed in the text. (C) An expanded contour plot of the symmetrical 1.0–3.3 ppm region. The lines connect cross peaks between CH_2 protons on the exocyclic ring.

a NOE to the 5.95 ppm sugar H1′ proton of A14 (boxed peak, Figure 5B) and the exocyclic CH_2 protons at 1.22, 2.87, and 3.06 ppm exhibit NOEs to the 5.75 ppm sugar H1′ proton of C13 (boxed peaks, Figure 5B).

The base and sugar proton chemical shifts of the X·A 9-mer duplex, pH 8.9, at 8 °C are listed in Table I. These assignments are based on the analysis of all regions of the NOESY spectrum and have been confirmed by analysis of two-dimensional COSY data.

Phosphorus Spectrum. The proton-decoupled ^{31}P spectrum of the X·A 9-mer duplex in D_2O buffer, pH 8.9, at 15 °C exhibits phosphorus resonances dispersed between −3.0 and −4.8 ppm (Figure 1C). Two phosphorus resonances are to low field and one phosphorus resonance is to high field of the −4.0 to −4.5 region.

pH-Dependent Conformational Equilibrium. Specific proton resonances (H8 proton of A14) provide resolvable markers for monitoring the pH-dependent conformational equilibrium between the X5(anti)·A14(anti) alignment at basic pH and the protonated X5(syn)·A14(anti) alignment at acidic pH in the X·A 9-mer duplex. The H8 proton of A14 resonates at 8.17 ppm in the basic pH form and at 8.47 ppm in the acidic pH form and is well resolved from other resonances in the 8.0–8.5 ppm region. The exchange between conformations is slow relative to the 0.30 ppm chemical shift separation so that the area under the H8 proton resonance of A14 in each state can be monitored as a function of pH. The transition exhibits a pK_a of ~7.6 for the pH-dependent conformational equilibrium at the X5·A14 lesion site in the X·A 9-mer duplex in aqueous solution. The pH titration curve is displayed in Figure 6.

NMR Distance Constraints. The volume integrals of the NOE cross peaks for the X·A 9-mer at pH 8.9 were measured and distance bounds established relative to cross peaks corresponding to the H6–H5 protons of cytidine (fixed 2.45-Å distance). The constraints, as defined by wide lower and upper bounds for the (G4-X5-G6)·(C13-A14-C15) segment at pH

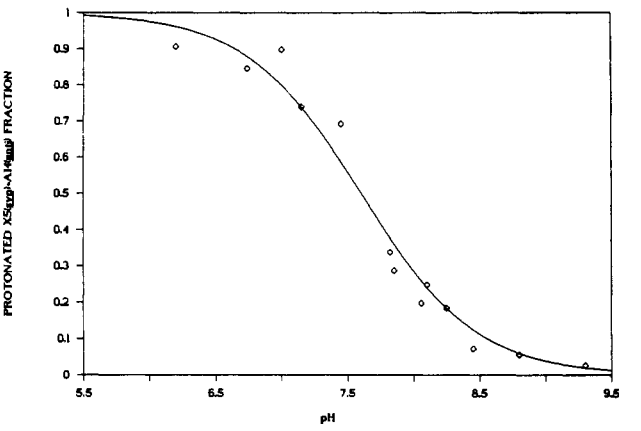

FIGURE 6: Plot of the fraction of the protonated X5(syn)·A14(anti) alignment as a function of pH. The plot is based on area measurements of the 8.47 ppm H8 resonance of A14 in the acidic pH conformation of the X·A 9-mer duplex. The pH values listed in the plot are corrected for the isotope effect and correspond to the pH meter reading plus 0.4 for samples measured in D_2O solution.

8.9, are summarized in Table IV. The distance bounds include base–sugar and sugar–sugar constraints within each nucleotide, base–base and base–sugar constraints between adjacent nucleotides, and constraints between the exocyclic CH_2 protons of X5 and the minor groove base and sugar H1′ protons (Table IV).

We previously reported on the NMR study of the X·A 9-mer at pH 5.8 (Kouchakdjian et al., 1989). Experimental distance constraints were also estimated for the entire X·A 9-mer duplex based on measurements of cross peak volume integrals in the NOESY spectra at pH 5.8. These constraints are also defined by wide lower and upper bounds and are summarized in Table SI (supplementary material). The distance bounds include constraints between the exocyclic CH_2 protons of X5 and the base protons of G4 on the same strand and A14 on the partner strand (Table SI), which help to define the pairing alignment at the X5·A14 lesion site.

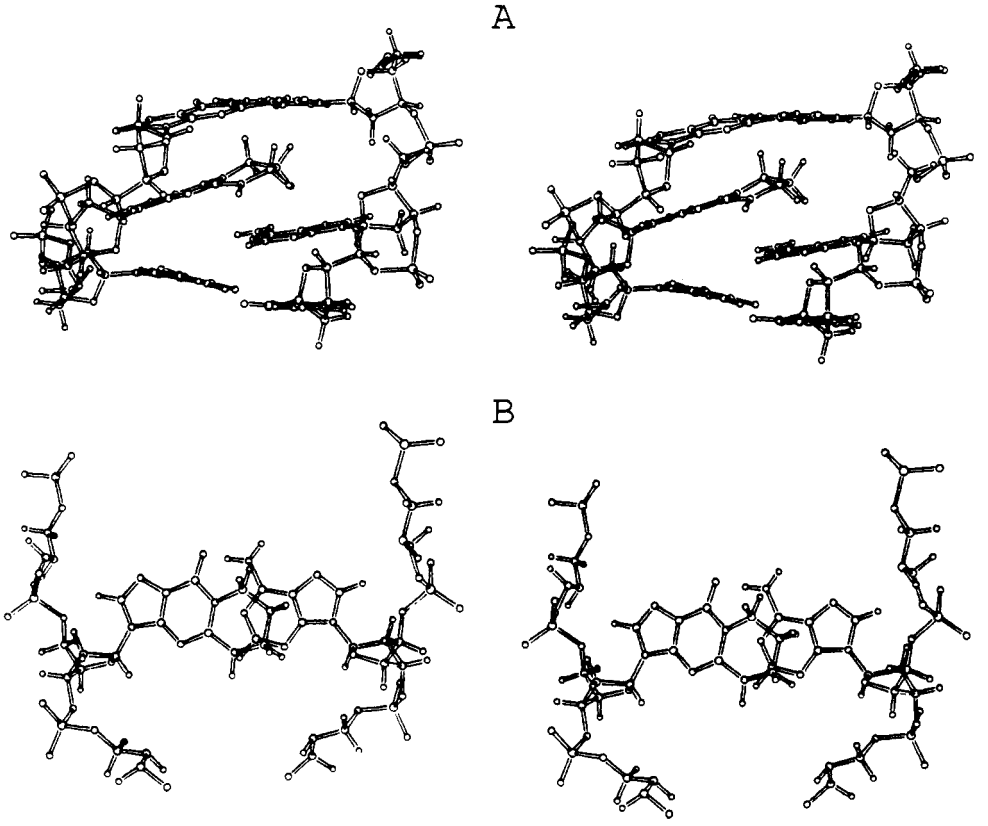

FIGURE 7: Stereopairs of (A) the (G4-X5-G6)·(C13-A14-C15) trinucleotide segment viewed normal to the helix axis and (B) the X5·A14 alignment viewed down the helix axis in the X·A 9-mer duplex at pH 8.9.

Energy Minimization Computations. The experimental distance bounds for the duplexes were incorporated as square-well potential constraints in the energy minimization algorithm of the XPLOR program. We included 145 distances for the conformation at basic pH and 188 distances for the acidic pH conformation. The starting alignment of X5 and A14 at the lesion site in the X·A 9-mer at basic pH is X5(anti) and A14(anti) with a severe steric clash between these bases in the center of the B-form DNA helix. This clash was relieved during the energy minimization run by van der Waals potential repulsion, with the realignment of X5 relative to A14 guided by the distance constraints from the observed NOEs between all the CH_2 protons of X5 and the H2 of A14, as well as by the NOEs between specific CH_2 protons of X5 and the sugar H1′ protons of C13 and A14 on the partner strand.

The starting alignment between X5 and A14 for the energy minimization run of the X·A 9-mer at acidic pH is protonated X5(syn)·A14(anti) based on the experimental data published previously (Kouchakdjian et al., 1989). Important constraints guiding the minimization computation are the observed NOEs between the exocyclic CH_2 protons and the H8 proton of adjacent G4, but not to the H8 proton of adjacent G6.

The final internal energy of the basic pH structure was 110 kcal/mol, while that for the conformation at pH 5.8 was 90 kcal/mol.

The energy-minimized (G4-X5-G6)·(C13-A14-C15) segment of the X·A 9-mer at basic pH is plotted in Figure 7A, while that for the X·A 9-mer at acidic pH is plotted in Figure 8A. These stereoviews normal to the helix axis emphasize the extent of structural distortion at the lesion site.

Stereoviews of the alignment of X5 and A14 at the lesion site as viewed down the helix axis are plotted in Figure 7B for the basic pH conformer and in Figure 8B for the acidic pH conformer.

The relevant interproton distances for the (G4-X5-G6)·(C13-A14-C15) segment in the basic pH conformer are listed in Table V and for the acidic pH conformer in Table SII (supplementary material).

Table IV: Proton–Proton Distance Constraints in the (G4–X5–G6)·(C13–A14–C15) Segment of the X·A 9-mer at pH 8.9

	intraresidue constraints on same strand (Å)			
	H6/H8–H1′	H6/H8–H2′	H6/H8–H2″	H1′–H2″
G4	2.7–4.5	1.9–3.8	2.0–3.5	*a*
X5	*b*	*a*	*a*	*b*
G6	2.7–4.5	1.9–3.7	2.3–4.0	2.2–3.9
C13	2.7–4.5	2.0–3.4	2.4–3.7	1.9–3.4
A14	2.7–4.5	2.2–3.8	2.2–3.4	*a*
C15	*a*	*a*	*a*	*a*

	interresidue constraints on same strand (Å)			
	H1′–H6/H8	H2′–H6/H8	H6/H8–H6/H8	H6/H8–H5/CH_3
T3–G4	2.5–4.1	2.5–4.1	3.4–5.6	
G4–X5	*a*	*a*	*b*	
X5–G6	*b*	*b*	*b*	
G6–T7	2.5–4.1	*b*	3.4–5.6	2.3–3.6
A12–C13	2.7–4.4	*a*	3.3–5.5	2.5–4.5
C13–A14	2.7–4.4	3.3–5.4	*b*	
A14–C15	2.7–4.4	*b*	3.4–5.6	*a*
C15–A16	*b*	*a*	*a*	

interresidue constraints on partner strands (Å)	
X5(1.22, 1.22 ppm CH_2)–A14(H2)	3.0–5.2
X5(1.84, 2.67, 2.87, 3.06 ppm CH_2)–A14(H2)	3.3–5.5
X5(1.22, 1.22 ppm CH_2)-C13(H1′)	3.3–5.5
X5(2.87, 3.06 ppm CH_2)-C13(H1′)	2.6–5.6
X5(1.22, 1.22 ppm CH_2)-A14(H1′)	3.4–5.6

[a] Overlap. [b] Very weak or absent.

DISCUSSION

General Considerations. The imino protons of deoxyguanosine and thymidine provide useful markers for deter-

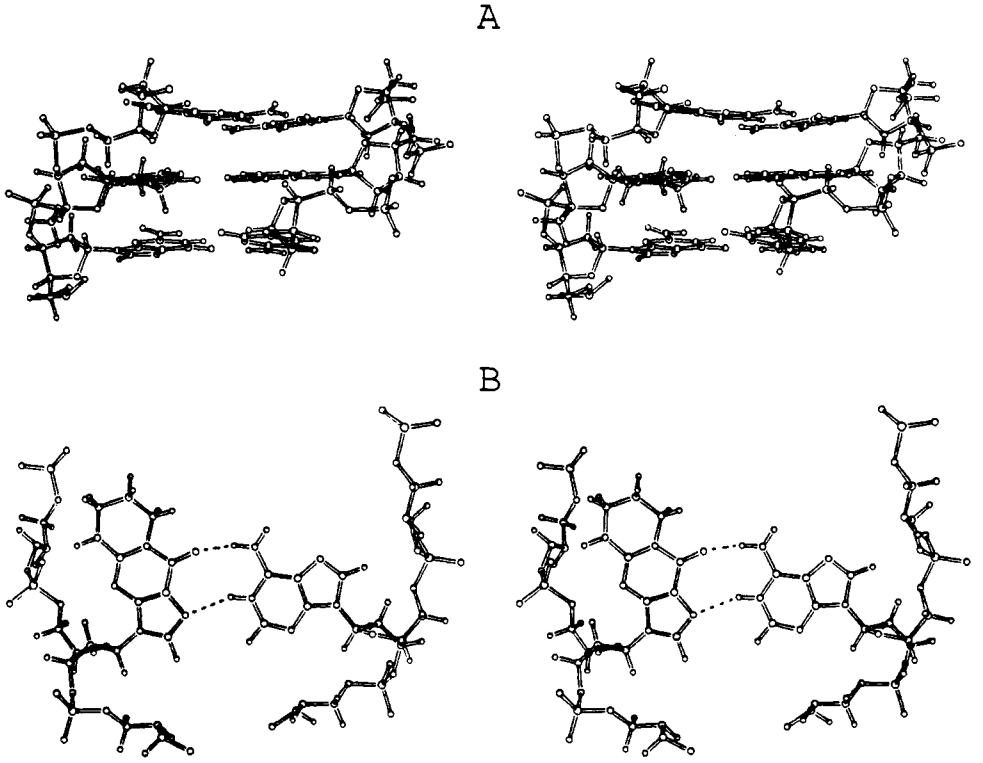

FIGURE 8: Stereopairs of (A) the (G4-X5-G6)·(C13-A14-C15) trinucleotide segment viewed normal to the helix axis and (B) the protonated X5·A14 pair viewed down the helix axis in the X·A 9-mer duplex at pH 5.8.

Table V: Proton–Proton Distances in the (G4–X5–G6)·(C13–A14–C15) Segment for the Basic pH Conformer of the X·A 9-mer at pH 8.9

	intraresidue distances on same strand (Å)			
	H6/H8–H1′	H6/H8–H2′	H6/H8–H2″	H1′–H2″
G4	3.9	2.4	3.6	2.5
X5	3.9	2.2	3.7	2.5
G6	3.9	2.3	3.5	2.5
C13	3.8	2.0	3.2	2.5
A14	3.9	2.1	3.1	2.5
C15	3.8	2.0	3.4	2.5

	interresidue distances on same strand (Å)			
	H1′–H6/H8	H2′–H6/H8	H6/H8–H6/H8	H6/H8–H5/CH_3
T3–G4	3.3	4.1	4.8	
G4–X5	2.7	4.2	5.2	
X5–G6	3.6	4.3	5.7	
G6–T7	3.0	4.7	5.5	4.2
A12–C13	3.5	4.5	5.0	3.9
C13–A14	4.8	5.3	6.1	
A14–C15	2.6	5.0	5.3	4.6
C15–A16	3.5	4.7	5.3	

interresidue distances on partner strands (Å)	
X5(1.22, 1.22 ppm CH_2)–A14(H2)	3.7, 4.9
X5(1.84, 2.67, 2.87, 3.06 ppm CH_2)–A14(H2)	3.2, 4.5, 4.7, 5.4
X5 (1.22, 1.22 ppm CH_2)–C13(H1′)	3.3, 4.4
X5(2.87, 3.06 ppm CH_2)–C13(H1′)	4.9, 5.0, 5.2, 5.2
X5(1.22, 1.22 ppm CH_2)–A14(H1′)	4.4, 5.5

mining the base-pairing characteristics of the X·A 9-mer duplex at pH 8.9. Each of the four thymidine imino protons displays NOEs to the deoxyadenosine H2 protons across the base pair (Figure 2B) establishing Watson–Crick hydrogen bonding for A2·T17, T3·A16, T7·A12, and A8·T11 base pairs. Similarly, the nonterminal deoxyguanosine imino protons of G4 and G6 each exhibit NOEs to the deoxycytidine amino protons on the partner strand (Figure 2B) consistent with formation of Watson–Crick G4·C15 and G6·C13 base pairs flanking the exocyclic X·A lesion site.

Helix handedness and base stacking may be evaluated by observing the directionality of NOE cross peaks in the NOESY spectrum of the X·A 9-mer duplex, pH 8.9, 8 °C in D_2O. The observed NOEs between the base (purine H8 or pyrimidine H6) protons and their own and 5′-linked sugar protons, NOEs between adjacent base protons in purine (3′–5′) pyrimidine (A2-T3, G6-T7, G10-T11, A12-C13, and A16-T17) steps, and NOEs between adenosine H2 protons and sugar H1′ protons on the same and the partner strand are characteristic of a right-handed helix with all bases being stacked into the duplex.

A14 at the Lesion Site. The A14 base lies across the helix axis from the exocyclic X5 adduct in the (G4-X5-G6)·(C13-A14-C15) segment so that NOEs involving the base and sugar protons of A14 provide structural constraints at the lesion site. Thus, the observed NOE between the H2 proton of A14 at the X5·A14 lesion site and the imino proton of the flanking Watson–Crick G4·C15 base pair (peak K, Figure 2b) but not the G6·C13 base pair establishes that A14 stacks into the helix and is directed toward the G4·C15 base pair. Furthermore, the magnitude of the NOE between the H8 and H1′ protons of A14 establishes an anti glycosidic torsional angle at A14. The 8.17 ppm chemical shift of the H8 of A14 is consistent with an unprotonated A14 ring in the X·A 9-mer duplex at pH 8.9.

The NMR parameters indicate an uncharacteristic structural perturbation immediately 3′ of the A14 nucleotide in the A14-C15-A16 segment. Several NOE cross peaks that are normally detected in unmodified DNA helices are very weak or absent in this segment. The expected cross peaks between the H6 proton of C15 and the H2′,H2″ protons of A14 (Figure 7A) and between the H8 proton of A16 and the H1′ proton of C15 (Figure 4B) have not been detected. Additionally, 5′ to the A14 lesion site, the NOE cross peak between the H8 of A14 and the H2′,H2″ of flanking C13 is weak (Figure 7A).

X5 at the Lesion Site. Despite the simplification of the NOESY data set in the ^{5}meC-modified X·A 9-mer duplex at pH 8.9 (Figure 5), the expected NOE between the H8 of X5

and its own H1′ proton is too weak to detect and hence the connectivity tracing is interrupted between G4 and G6 (Figure 5A). These data rule out a syn orientation at X5 since a strong NOE is predicted between the H8 proton of X5 and its own sugar H1′ proton for this orientation (Patel et al., 1982). Further support for this conclusion is based on the observed NOE detected between the H8 and H2′ protons of X5 (cross peak designated X5 in Figure 5A) in the X·A 9-mer at pH 8.9. The NOE patterns also establish a perturbation in the X5-G6 step since no NOEs are detected between the H8 of G6 and the H1′ (Figure 3A) and the H2′,H2″ protons (Figure 5A) of X5. The absence of NOEs to the H1′ proton of X5 may reflect an increased line width for this proton in the X·A 9-mer duplex at pH 8.9.

The distance connectivities involving the exocyclic CH_2 protons of X5 help align the exocyclic ring within the (G4-X5-G6)·(C13-A14-C15) segment of the X·A 9-mer duplex at pH 8.9. The weak NOE between the central exocyclic CH_2 proton of X5 at 1.22 ppm and the imino proton of the flanking G6·C13 base pair (peak M, Figure 2C) but not the G4·C15 base pair establishes that the glycosidic torsion angle of X5 is in the anti range and that X5 is directed toward the G6·C13 base pair. Moreover, weak NOEs between the 1.22 ppm exocyclic CH_2 protons and the sugar H1′ protons of C13 and A14 (boxed peaks, Figure 5B) demonstrate that the exocyclic ring of X5 must be directed toward the C13-A14 segment on the partner strand.

X5(anti)·A14(anti) Alignment. An important set of NOEs for alignment of X5 and A14 at the lesion site are those detected between all the resolved exocyclic CH_2 protons and the 7.62 ppm H2 proton of A14 (boxed peaks, Figure 5A) in the X·A 9-mer at pH 8.9. These NOEs are of medium intensity and align the exocyclic ring of X5 in close proximity to A14 at the lesion site.

The experimental NMR data establish that both X5 and A14 are in the anti range and that the exocyclic propano linkage of X5 is directed toward the partner strand.

Distance Constraints and Energy Minimization. The interproton distances for the (G4-X5-G6)·(C13-A14-C15) segment of the energy-minimized conformation of the X·A 9-mer at pH 8.9 (Table V) are, as expected, within the experimentally determined bounds (Table IV) based on the NOESY data sets. We do note, however, that the short distances of 2.7 Å between the H8 of X5 and the H1′ of G4 and 2.6 Å between the H6 of C15 and the H1′ of A14 for the computed conformation (Table V) would result in stronger NOE cross peaks than observed experimentally (Figure 4). The wide range of the experimental distance bounds (Table IV) implies that the conformation drawn in Figure 7 represents a low-resolution view of the X5·A14 lesion site and its flanking base pairs in solution. We refrain, therefore, from a detailed listing of the helical parameters. Such a study requires tighter distance constraints deduced either from the measurement of the initial buildup of the NOE or alternately from a comparison of calculated and experimental NOESY spectra. This limitation notwithstanding, our proposed alignments of X5-(anti)·A14(anti) at basic pH (Figure 7) and protonated X5-(syn)·A14(anti) at acidic pH (Figure 8) represent the first three-dimensional structures defining the accommodation of bulky adducts into DNA oligomer duplexes in solution.

Basic pH Conformation. The novel alignment of X5 and A14 at the lesion site in the X·A 9-mer duplex at pH 8.9 (Figure 7) was unexpected and provides new insights into the accommodation of bulky nonplanar ligands into the interior of DNA duplexes. First, X5 and A14 are not stabilized by hydrogen bonding but rather through stacking following partial intercalation between bases on the partner strand. The observed mutual intercalation of X5 between C13 and A14 and of A14 between G4 and X5 is reminescent of similar structural motifs observed in the crystal structure of transfer RNA (Jack et al., 1976; Holbrook et al., 1978). Second, there is a selection for one of the two possible simultaneous partial intercalation conformations with X5 directed toward the G6·C13 base pair and A14 directed toward the G4·C15 base pair rather than the reverse alignment. Third, the flanking G4·C15 and G6·C13 base pairs retain Watson–Crick alignment but are separated by a larger distance due to the partial stacking of opposing X5 and A14 at the lesion site at basic pH.

Acidic pH Conformation. The protonated X5(syn)·A14-(anti) alignment at acidic pH (Figure 8) incorporates all the features discussed in our earlier paper (Kouchakdjian et al., 1989). The syn glycosidic torsion angle at X5 positions the exocyclic ring in the major groove such that its Hoogsteen edge can pair with the Watson–Crick edge of N1-protonated A14 through two hydrogen bonds.

pH-Dependent Conformational Parameters at the Lesion Site. It is instructive to compare the NMR parameters for the trinucleotide segment centered about the lesion site for the high-pH and low-pH conformations of the X·A 9-mer duplex. The exchangeable and nonexchangeable proton chemical shift differences for the (G4-X5-G6)·(C13-A14-C15) segment between pH 5.8 and pH 8.9 are listed in Table II. The chemical shifts of the exocyclic CH_2 protons of X5 in the X·A 9-mer duplex at pH 5.8 and pH 8.9 are listed in Table III.

The 1,N^2-propanodeoxyguanosine at the X5·A14 lesion site adopts a syn orientation about the glycosidic bond at pH 5.8 and an anti orientation at pH 8.9. Thus, the exocyclic adduct protrudes into the major groove away from the helix axis in the conformation at pH 5.8 while it is closer to the helix axis and directed toward the partner strand in the conformation at pH 8.9. This is reflected in the exocyclic CH_2 proton chemical shifts, which resonate to high field at basic pH (Table III) as a consequence of improved stacking of the exocyclic ring with adjacent base pairs.

The amino protons of A14 resonate at 10.18 and 8.28 ppm in the X·A 9-mer duplex at pH 5.8 with the downfield chemical shift values reflecting protonation of the adenosine ring in the protonated X5(syn)·A14(anti) pair at low pH. By contrast, these downfield shifts are absent in the X·A 9-mer duplex at pH 8.9, consistent with a neutral A14 at the X5(anti)·A14-(anti) pair at basic pH. Similarly, protonation of the adenosine ring at acidic pH results in downfield shifts of the H8 and H2 protons of A14 at the X5·A14 lesion site (Table II).

The conformational dependence on pH of the exocyclic deoxyguanosine adduct opposite deoxyadenosine has provided valuable insights toward helping us understand the role of protonation in base pairing. For normal Watson–Crick A·T base pairs, the deoxyadenosine is not protonated at pH 5.8. In the case of A14 in the X·A 9-mer duplex, however, deoxyadenosine becomes fully protonated at pH 5.8. At this pH, the protonated deoxyadenosine base (A14) provides two hydrogen bond donors, and these are accommodated by the partner exocyclic deoxyguanosine base (X5) in a syn orientation through formation of two Hoogsteen-type hydrogen bonds. Upon loss of protonation of the deoxyadenosine at high pH, the possible hydrogen bond donors on this base are reduced to one and the exocyclic deoxyguanosine base adopts an anti conformation. The resulting X5(anti)·A14(anti) alignment does not involve base pairing and is stabilized primarily by hydrophobic stacking interactions. The present study estab-

lishes the interplay between hydrogen-bonding, base-protonation, and base-stacking contributions to helical stability at lesion sites in DNA duplexes.

Conformational Equilibrium. The equilibrium between the basic pH X5(anti)·A14(anti) conformer and the acidic pH protonated X5(syn)·A14(anti) conformer exhibits a pK_a of ~7.6 (Figure 6). This value can be contrasted with a pK_a of ~5.5 for the conformational equilibrium between the neutral pH G(anti)·A(anti) pair and acidic pH protonated G(syn)·A(anti) pair for this purine–purine mismatch embedded in DNA duplexes [Gao and Patel (1988) and unpublished results].

The conformational equilibrium between the X5(anti)·A14(anti) alignment at basic pH and the protonated X5(syn)·A14(anti) alignment at acidic pH is in the slow-exchange limit relative to the 0.3 ppm separation of the H8 proton of A14 between states. This translates into an interconversion rate that is less than 900 s^{-1} ($k < 2\pi\delta\nu$, where $\delta\nu$ is 150 Hz).

Summary. We are attempting to define the molecular basis of mutagenic and carcinogenic potential associated with exocyclic adduct formation in DNA. Cyclic adduct formation induces pK_a and hydrophobicity changes and altered pairing possibilities at the lesion site. Our studies on 1,N^2-propanodeoxyguanosine, a stable analogue of the adduct resulting from the action of acrolein on deoxyguanosine, have provided the first insights into potential alignments for accommodating bulky exocyclic adducts in DNA helices. The NMR studies have focused on 1,N^2-propanodeoxyguanosine (X) positioned opposite deoxyadenosine in the center of a deoxynonanucleotide duplex and have defined the pairing alignments as a function of pH.

Previous studies on G·A mismatches have established that the pairing alignments are dependent on pH both in solution (Gao & Patel, 1988) and in the crystalline state (Brown et al., 1989). A similar pH-dependent structural transition has been detected at the central X·A lesion site in the deoxynonanucleotide duplex. The measured pK_a of approximately 7.6 for the pH-dependent transition at the X·A lesion site contrasts with the pK_a of approximately 5.5 for the pH-dependent transition at the G·A mismatch site.

The high-pH state has been characterized as X(anti)·A(anti) at the exocyclic lesion site (this study) and G(anti)·A(anti) at the mismatch site (Kan et al., 1983; Patel et al., 1984; Prive et al., 1987). The G(anti)·A(anti) mismatch is stabilized by two hydrogen bonds and results in a small perturbation in the helix associated with a larger separation between C1′ carbons across the pair. Stacking is maintained throughout the helix including the G·A mismatch and its flanking base pairs. Base pairing is precluded at the X(anti)·A(anti) lesion site, with both X and A partially intercalating between stacked bases on partner strands. The resulting perturbation increases the separation between intact flanking base pairs and results in a pronounced helical disruption that may be recognized and corrected for by repair enzymes.

By contrast, the low-pH alignment has been characterized as protonated X(syn)·A(anti) at the lesion site with minimal disruption in the helical parameters (Kouchakdjian et al., 1989). The bulky exocyclic group is located in the major groove and the pairing alignment is stabilized by two hydrogen bonds following protonation of the N1 of deoxyadenosine.

Our studies establish a pH-dependent alignment of 1,N^2-propanodeoxyguanosine opposite deoxyadenosine in the interior of DNA helices, which reflects the interplay between hydrogen bonding and hydrophobic interactions modulated by the pH of the solution.

Supplementary Material Available

Tables of experimental (Table SI) and computed (Table SII) proton–proton distances in the (G4-X5-G6)·(C13-A14-C15) segment for the acidic pH conformer of the X·A 9-mer at pH 5.8 and figures showing a one-dimensional NOE difference spectrum of the X·A 9-mer in H_2O, pH 8.9 (Figure S1), the phase-sensitive NOESY contour plot of the X·A 9-mer in D_2O, pH 8.9 (Figure S2), stacked plots of 250- and 50-ms NOESY contour plots of the base proton to H1′ proton region of the X·A 9-mer in D_2O (Figure S3), and a contour plot of the proton-detected proton–phosphorus heteronuclear COSY experiment on the X·A 9-mer in D_2O, pH 8.9 (9 pages). Ordering information is given on any current masthead page.

References

Basu, A. K., & Essigmann, J. M. (1988) *Chem. Res. Toxicol. 1*, 1–18.

Brown, T., Leonard, G. A., Booth, E. D., & Chambers, J. (1989) *J. Mol. Biol. 207*, 455–457.

Chung, F. L., Young, R., & Hecht, S. S. (1984) *Cancer Res. 44*, 990–995.

Gao, X., & Patel, D. J. (1988) *J. Am. Chem. Soc. 110*, 5178–5182.

Grollman, A. P. (1989) *Proc. Am. Assoc. Cancer Res. 30*, 682.

Holbrook, S. R., Sussman, J. L., Warrant, R. W., & Kim, S. H. (1978) *J. Mol. Biol. 123*, 631–660.

Jack, A., Ladner, J. E., & Klug, A. (1976) *J. Mol. Biol. 108*, 619–649.

Kan, L. S., Chandrasegaran, S., Pulford, S. M., & Miller, P. S. (1983) *Proc. Natl. Acad. Sci. U.S.A. 80*, 4263–4265.

Kouchakdjian, M., Marinelli, E., Gao, X., Johnson, F., Grollman, A., & Patel, D. J. (1989) *Biochemistry 28*, 5647–5657.

Live, D., Davis, D. G., Agosta, W. C., & Cowburn, D. (1984) *J. Am. Chem. Soc. 106*, 1939.

Marinelli, E. R., Johnson, F., Iden, C. R., & Yu, P. L. (1990) *Chem. Res. Toxicol. 3*, 49–58.

Norman, D., Abuaf, P., Hingerty, B. E., Live, D., Grunberger, D., Broyde, S., & Patel, D. J. (1989) *Biochemistry 28*, 7462–7476.

Patel, D. J., Kozlowski, S. A., Nordheim, A., & Rich, A. (1982), *Proc. Natl. Acad. Sci. U.S.A. 79*, 1413–1417.

Patel, D. J., Kozlowski, S. A., Ikuta, S., & Itakura, K. (1984) *Biochemistry 23*, 3207–3217.

Prive, G. G., Heinemann, U., Kan, L. S., Chandrasegaran, S., & Dickerson, R. E. (1987) *Science 238*, 498–504.

Shapiro, R. (1969) *Ann. N.Y. Acad. Sci. 163*, 624–630.

Singer, B., & Grunberger, D. (1983) in *Molecular Biology of Mutagens and Carcinogens*, Plenum Press, New York.

Singer, B., & Bartsch, H. (1986) *The Role of Cyclic Nucleic Acid Adducts in Carcinogenisis and Mutagenesis, No. 70*, IARC Scientific Publications, Lyon, France.

Sklenar, V., & Bax, A. (1987) *J. Am. Chem. Soc. 109*, 7525.

Sklenar, V., Miyashiro, H., Zon, G., Miles, H. T., & Bax, A. (1986) *FEBS Lett. 208*, 94–98.